Boltzmann Solver with Adaptive Mesh in Velocity Space

Vladimir I. Kolobov[a], Robert R. Arslanbekov[a], and Anna A. Frolova[b]

[a]*CFD Research Corporation,*
215 Wynn Dr, Huntsville, AL, 35803, USA
[b]*Dorodnicyn Computing Centre of the Russian Academy of Sciences,*
Vavilova Str., 40, Moscow, 119333, Russia

Abstract. We describe the implementation of direct Boltzmann solver with Adaptive Mesh in Velocity Space (AMVS) using quad/octree data structure. The benefits of the AMVS technique are demonstrated for the charged particle transport in weakly ionized plasmas where the collision integral is linear. We also describe the implementation of AMVS for the nonlinear Boltzmann collision integral. Test computations demonstrate both advantages and deficiencies of the current method for calculations of narrow-kernel distributions.

Keywords: Rarefied Gas Dynamics, Boltzmann kinetic equation, charged particles, octree Cartesian mesh, adaptive mesh in velocity space, weakly ionized plasma
PACS: 51.10.+y, 52.25.Dg, 52.30.-q

INTRODUCTION

Direct Boltzmann solvers are increasingly being used as alternative to statistical (DSMC) methods for simulations of rarefied gases and plasmas. They are very attractive for hybrid codes that use kinetic and hydrodynamic models in different parts of computational domain [1]. Direct methods introduce mesh in velocity space (in addition to mesh in physical space) and solve kinetic equations on this mesh. The efficiency of such solvers can be increased by using adaptive mesh in velocity space. Advantages have already been demonstrated for Vlasov solvers [2]. It is believed that adaptive mesh is a must for multi-dimensional kinetic simulations of hypersonic flows with deterministic (non-statistical) methods.

In this paper, we describe the implementation of Boltzmann solver with Adaptive Mesh in Velocity Space (AMVS) using quad/octree Cartesian mesh. Cartesian mesh is particularly attractive for this purpose because there are no complex boundaries in velocity space. We demonstrate the benefits of the AMVS technique for the charged particle transport in weakly ionized plasmas where the collision integral is linear. We also describe the implementation of AMVS for the nonlinear Boltzmann collision integral describing elastic collisions among neutral gas particles. Test computations demonstrate both advantages and deficiencies of the current method for calculations of narrow-kernel distributions.

DIRECT BOLTZMANN SOLVERS

The numerical solution of the Boltzmann equation can be split into advection in physical space

$$\frac{\partial f_i}{\partial t} + \nabla_r \cdot \left(\boldsymbol{\xi}_i f_i\right) = 0 \tag{1}$$

and transport in velocity space due to forces and collisions

$$\frac{\partial f_j}{\partial t} + \nabla_\xi \cdot \left(\mathbf{a}_j f_j\right) = S(f) \tag{2}$$

Here $\boldsymbol{\xi}$ is the particle velocity, **a** is the acceleration vector, and *S* is the collision integral. We used a tree-based dynamically adaptive Cartesian grid to solve Eq (1) by traditional finite volume CFD techniques [1]. Similar grid can be generated in velocity space to solve Eq (2).

We have used the octree/quadtree data structure of GFS [3] to implement the numerical solution of Eq (2) with adaptive mesh in velocity space. The force part was implemented using the finite volume formulation with second-order accuracy in time and in (2D and 3D) velocity space. The collision integral has the following form:

$$S(\boldsymbol{\xi}) = N \int_{S^2} d\boldsymbol{\omega} \int_{R^3} \left(f(\boldsymbol{\xi}_1') f(\boldsymbol{\xi}') - f(\boldsymbol{\xi}_1) f(\boldsymbol{\xi}) \right) g \sigma(g, \chi) d\boldsymbol{\xi}_1 = -\nu(\boldsymbol{\xi}) f(\boldsymbol{\xi}) + G \quad . \tag{3}$$

Here ν is the collision frequency, *G* is the inverse collision integral, $g = |\boldsymbol{\xi}_1 - \boldsymbol{\xi}|$ is the relative velocity of the colliding particles, $\boldsymbol{\omega}$ is a vector on a unit sphere S^2 in velocity space, and $d\boldsymbol{\omega}$ is an element of the area of the surface of this sphere, $\sigma(g, \chi)$ is the differential collision cross section. The calculation of this integral constitutes the main difficulty of solving the Boltzmann equation. We have explored several types of collision integrals.

LINEAR COLLISION INTEGRALS

The collision integral (3) can be simplified when the density of species of interest is much lower that the density of background gas species. This is an important case of charged particle transport in weakly ionized plasmas.

Ions Moving in a Parent Gas: Charge Exchange Collisions

We first consider the charge-exchange collisions of ions with the parent gas atoms, when the collision integral can be written in the form [4]:

$$S_i = N \int_{R^3} \left[f(\boldsymbol{\xi}_1) \varphi(\boldsymbol{\xi}) - f(\boldsymbol{\xi}) \varphi(\boldsymbol{\xi}_1) \right] |\boldsymbol{\xi} - \boldsymbol{\xi}_1| \, \sigma_{ex} d\boldsymbol{\xi}_1 \tag{4}$$

where $\varphi(\xi)$ is a Maxwellian velocity distribution of the background gas atoms with density *N* and temperature *T*, σ_{ex} is a charge exchange collision cross-section.

Consider ions with a mass *M* injected in DC electric field *E* and experiencing charge-exchange collisions with a steady background gas. The charge exchange collisions cannot change the velocity distribution orthogonal to the electric field direction. So, the velocity distribution is of the form $f(\boldsymbol{\xi}) = \Phi(\xi_\perp) F(\xi_x)$. The distribution function $F(\xi_x)$ evolves in time until a steady state is reached. The analytical expression for the steady state distribution $F(\xi_x)$ can be obtained in the form

$$F(\xi_x) = C \exp\left(-\frac{NM}{eE} \int_0^{\xi_x} \xi_x \sigma_{ex}(\xi_x) d\xi_x \right) \tag{5}$$

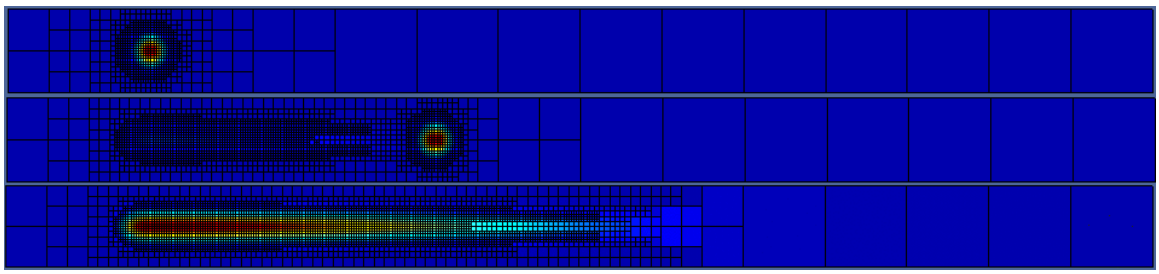

FIGURE 1. Ion distribution function at three moments in time: initial, intermediate and final.

Figure 1 shows results of the numerical solution of Eq (2) with the collision integral (4) using adaptive mesh in velocity space. The applied force has a magnitude of 4 and the charge-exchange collision-frequency is equal to 1. Figure 1 shows the calculated ion distribution function at three moments in time: initial, intermediate and final. One can see that the grid dynamically adapts to the features of the distribution function in velocity space. Figure 2 shows the distribution functions along the $\xi_y = 0$ line for different time moments (left) and distribution functions along ξ_x = const lines. One can see that the calculated steady-state distribution function compares well with the analytical solution. In the ξ_y-direction, the distribution function remains a Maxwellian with the temperature of the source function (which represents cold, motionless atoms on which charge-exchange occurs).

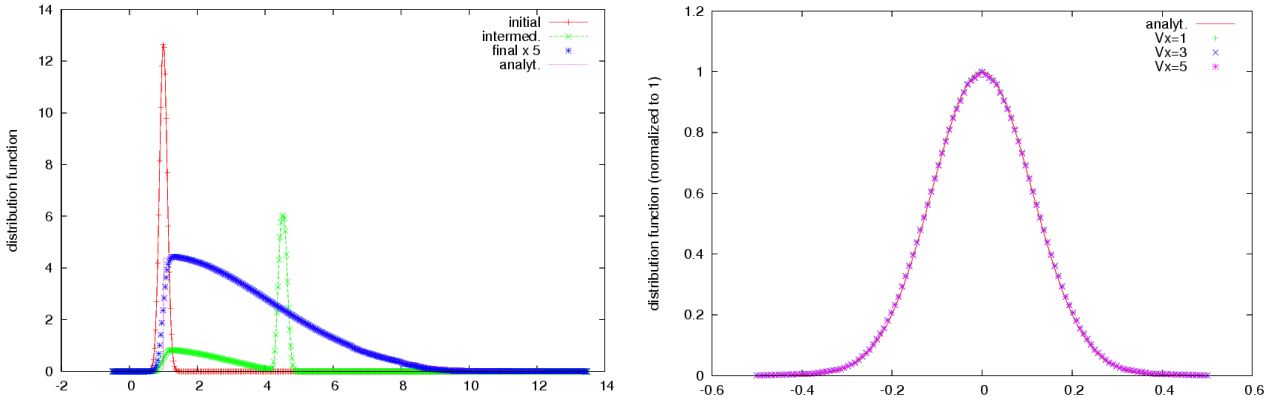

FIGURE 2. Ions distribution functions along $\xi_y = 0$ line for different time moments (left) and distribution functions vs ξ_y lines for different ξ_x positions (right).

Lorentz gas

A gas mixture with atoms of disparate mass is called a Lorentz gas. In such a mixture, the relaxation processes occur in several stages with different time scales. For elastic collisions of light particles with heavy particles, the collision integral consists of two terms. The first term describes momentum relaxation [5]:

$$S_0 = N\xi \int_{S^2} \sigma(\xi, |\Omega - \Omega'|)\left[f(\xi, \Omega') - f(\xi, \Omega) \right] d\Omega \qquad (6)$$

where $\boldsymbol{\Omega}$ is a velocity angle on a unit sphere S^2, and $\boldsymbol{\xi} = \xi\boldsymbol{\Omega}$. The differential collision cross section depends on the initial speed and the angle $\theta = \arccos(\boldsymbol{\Omega} \cdot \boldsymbol{\Omega}')$ between the initial and final particle velocity. When the scattering is close to isotropic $\sigma(\xi, |\Omega - \Omega'|) = \sigma(\xi)$, the integral (6) is further simplified:

$$S_0 = -\nu[f(\xi, \Omega) - \int_{S^2} f(\xi, \Omega) d\Omega] \qquad (7)$$

where $\nu = N\xi\sigma(\xi)$ is the collision frequency. We have implemented the collision integral (7) using a special technique to correctly treat the leaps of particles from one velocity cell to another for non-uniform and unstructured grids.

Figure 3 illustrates the relaxation process described by Eq (2) with collision integral (7). The initial velocity distribution function has a non-zero mean velocity, V_{0x} = 0.3, and a temperature T = 0.005 (in units of thermal velocity). Figure 3 shows the computational mesh, 2D contours of the velocity distribution function at different times, and a 3D surface of constant VDF. The corresponding macroparameters are shown in Figure 4. The density is conserved with machine precision. The mean velocity drops to zero in about two collisional times. The temperatures T_x and T_y evolve towards a single temperature within the same time scale.

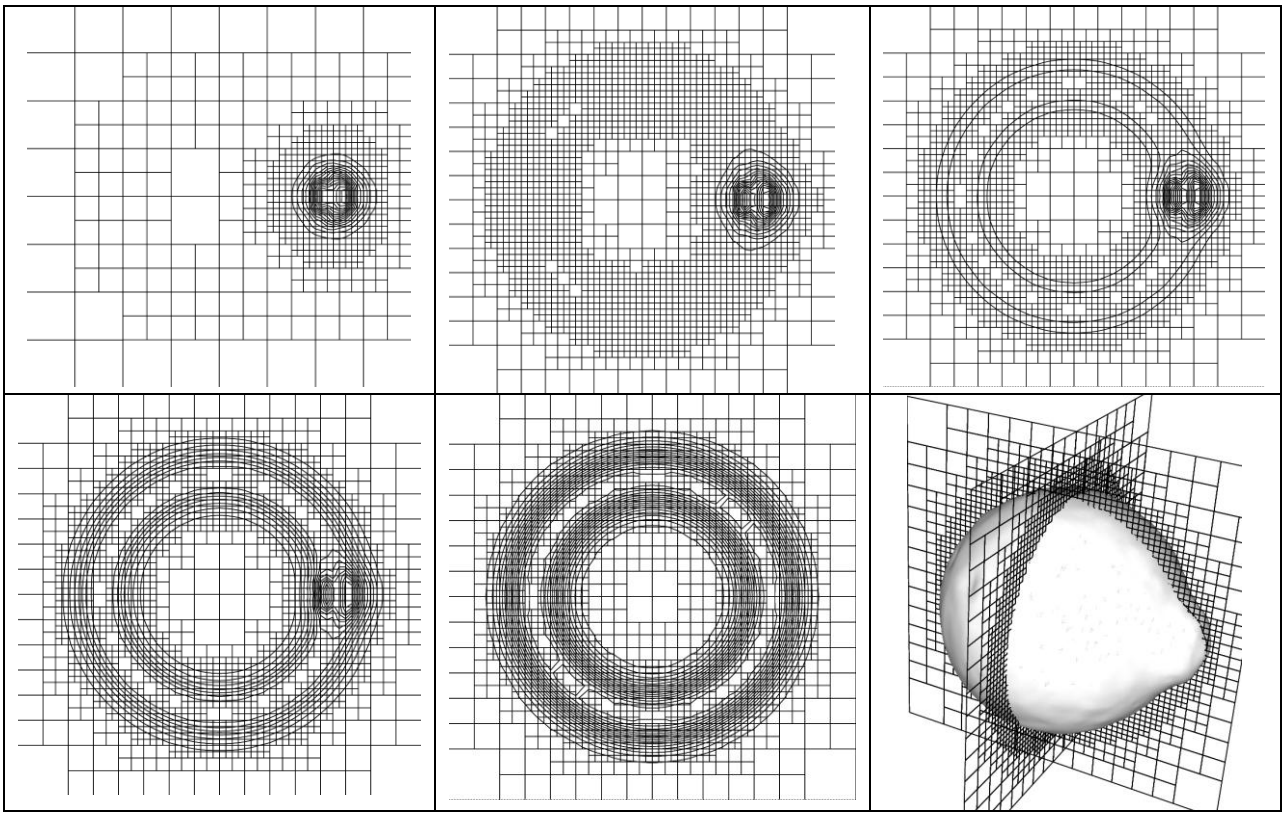

FIGURE 3. The computational grid and contours of the velocity distribution functions at different times under the action of collisions described by the integral (7).

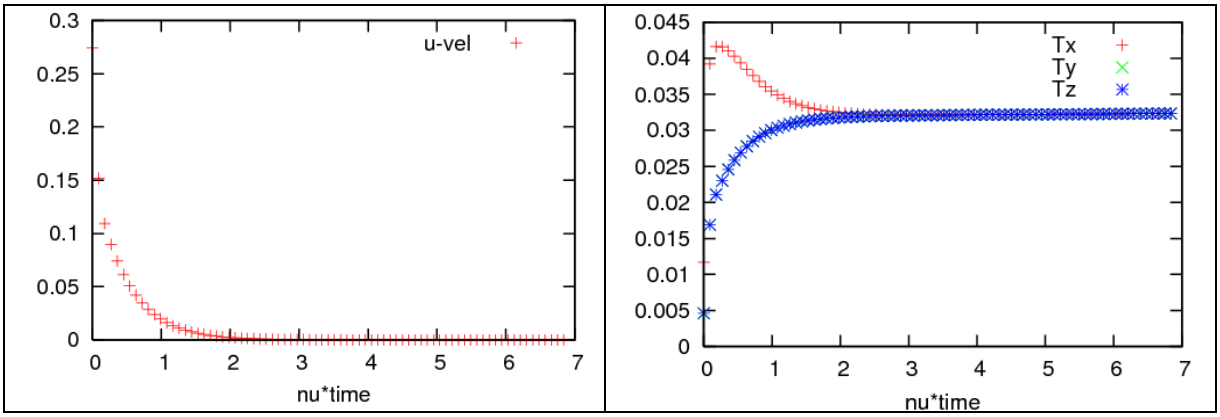

FIGURE 4. Time evolution of macro-parameters of a distribution function with initial non-zero velocity.

NON-LINEAR COLLISION INTEGRALS

Numerical algorithms for calculation of the nonlinear Boltzmann collision integral (3) for a uniform static mesh in velocity space were described in [1]. They include the Node to Node (NtN) method, Cheremisin method, and the Node to Closest Node (NtCN) method. For calculation of the collision integral (3) on a dynamically adaptive Cartesian mesh in velocity space we used the following procedure. If velocities of direct and inverse collisions belong to cells with the same refinement level, their contributions to the collision integral was accounted for by the Cheremisin method. If they belong to cells with different refinement level, their contribution was accounted for by the NtCN method applicable for non-uniform mesh.

The NtCN procedure for accounting inverse collisions introduces errors in conservation of mass, momentum and energy. In order to eliminate these errors, we introduce a correction to the collision frequency using the method of least squares:

$$\nu^*(\xi) = (1 + a_0 + a_1\xi_x + a_2\xi_y + a_3\xi_z + a_4(\xi_x^2 + \xi_y^2 + \xi_z^2))\nu(\xi)\,.$$

If the polynomial correction $P = (a_0 + a_1\xi_x + a_2\xi_y + a_3\xi_z + a_4(\xi_x^2 + \xi_y^2 + \xi_z^2) < -1$, we introduce a correction to the inverse integral $G^*(\xi) = G(\xi) - P\nu(\xi)f(\xi)$, where the coefficients a_i are defined from the collision invariants. For calculations with AMVS, we interpolated the velocity distribution function to the current mesh. This interpolation procedure ensures the conservation of density but can introduce misbalances in the temperature and impulses. These misbalances in the moments introduced by the dynamic mesh adaptation can be partially accounted for by corrected collision frequency.

For evaluation of the eight-dimensional integrals, the Korobov sequences [6] were applied. The Korobov's points in a s-dimensional hypercube are defined as

$$x_{r\nu} = \left\{\nu a_r^{p_\nu} / p\right\}, \qquad r = 1,2,...,s, \quad \nu = 1,2,..., p-1 \tag{8}$$

where p is a prime number, $a_r^{p_\nu}$ are precalculated integer coefficients, and the brace denotes the reminder on dividing an integer by an integer. The velocity grid points closest to the selected Korobov's points are taken as the selected velocity grid points. The accuracy of this procedure is estimated as $O((\ln N_c)^{\alpha s} / N_c^{\alpha})$, where the exponent $\alpha \geq 1$ depends on the smoothness of the integrated function (for a piecewise-constant function, $\alpha = 1$). The above error is less than the estimated error of the Monte Carlo method for calculating multi-dimensional integrals.

Figure 5 illustrates the collisional relaxation of an initial bi-Maxwellian velocity distribution function $f \sim \exp\left(-\left((\xi_x \pm u)^2 + \xi_y^2 + \xi_z^2\right)/T\right)$, calculated in a unit box with u = 0.225, and T = 0.004. One can observe that a "cavern" is formed at early stages of relaxation, as previously reported by Beylich [7].

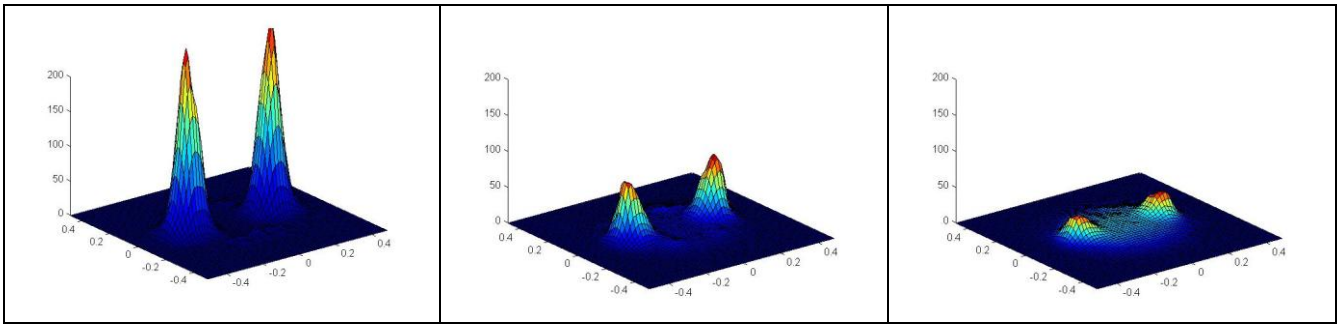

FIGURE 5. Relaxation of bi-Maxwellian distribution towards a single Maxwellian in the plane $\xi_z = 0$. Hard Sphere collision model.

Figure 6 shows the computational mesh and contours of the VDF in the plane $\xi_z = 0$. Mesh adaptation is based on the value of $|-\nu(\xi_i)f(\xi_i) + G(\xi_i)|$. At early stages, non-uniform mesh was specified based on knowledge of collision dynamics. Figure 7 shows the time dependence of temperatures and mean velocities during the relaxation process.

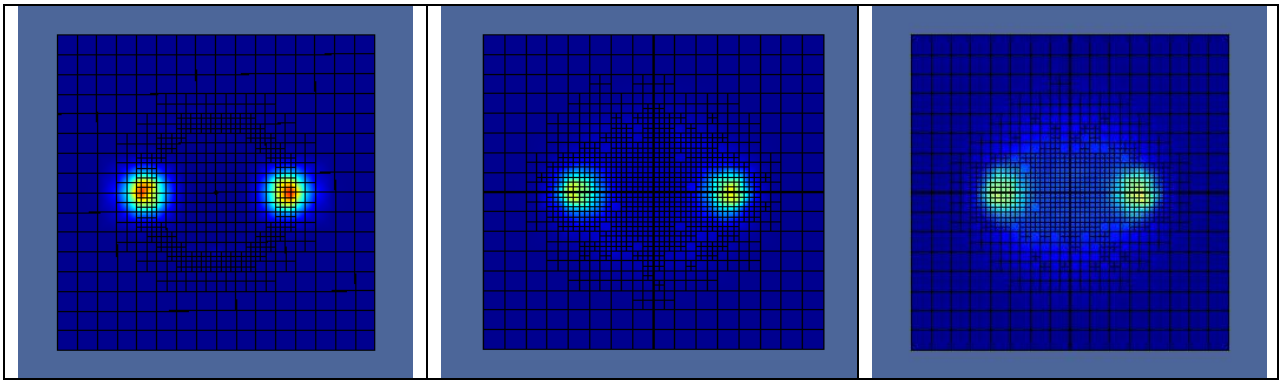

FIGURE 6. Computational mesh and VDF countours (color) in the $\xi_z = 0$ plane for the conditions as in Figure 5 .

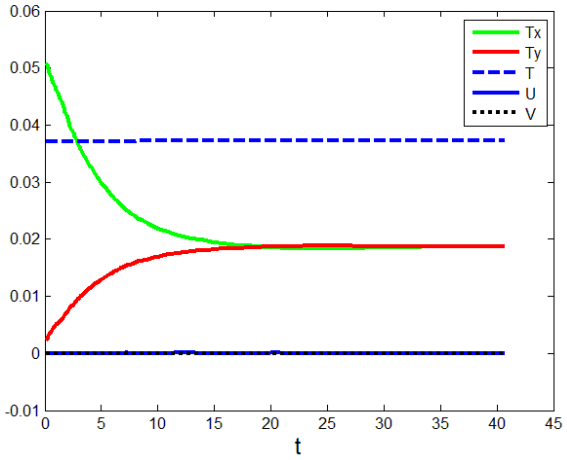

FIGURE 7. Time dependence of macroparameters during the relaxation process.

The methodology described above allowed us for the first time to calculate the Boltzmann collision integral with dynamically adaptive Cartesian mesh in velocity space. Test computations have demonstrated both the advantages and deficiencies of the method for calculations of narrow-kernel distributions. The main problem limited the efficiency of the method consists of the uniform distribution of the Korobov's nodes, which does not account for the refinement of the mesh.

ACKNOWLEDGMENTS

This work was partially supported by the AFOSR STTR project FA9550-10-C-0053 monitored by Dr John Schmisseur.

REFERENCES

[1] V.I. Kolobov, R.R. Arslanbekov, V.V. Aristov, A.A. Frolova, S.A. Zabelok, J. Comput. Phys. 223, 589 (2007)
[2] M.Mehrenberger, et al, Nuclear Instruments and Methods in Physics Research A 558 (2006) 188
[3] http://gfs.sourceforge.net
[4] B.M.Smirnov, Physics of Weakly-Ionized Gases: Problems and Solutions (1982)
[5] P.P.J.M.Schram, *Kinetic Theory of Gases and Plasmas*, Springer (1991)
[6] N.N.Korobov, Trigonometric sums and their applications, Mir, Moscow (1998)
[7] A.E.Beylich, Phys. Fluids 14, 2683 (2002)